Numerical Experiments Performed on the Imperial College Plasma Focus Machine: Dependence on Deuterium Pressure

Arwinder Singh[1,*], Saw Sor Heoh[2, 3] and Sing Lee[1, 2, 3, 4]

[1]*INTI International University, Persiaran Perdana BBN, Putra Nilai, 71800 Nilai, Negeri Sembilan, Malaysia*
[2]*Nilai University, No 1, Persiaran University, Putra Nilai, 71800 Nilai, Negeri Sembilan, Malaysia*
[3]*Institute for Plasma Focus Studies, 32 Oakpark Drive, Chadstone, VIC3148, Australia.*
[4]*University of Malaya, Kuala Lumpur, Malaysia.*

* *arwinders.jigiris@newinti.edu.my*

(Received: 21 April 2016; published 6 August 2016)

Abstract. In this paper, we use Lee's 5 phase model code to configure the Imperial College Plasma focus machine operating in the pressure (P_0) range from 0.5 Torr to 6 Torr to obtain the relationship between axial speed v_a, radial shock speed v_s, piston speed v_p and pinch temperature with P_0 as follows:

$$v_a \approx 14\,P_0^{-0.42},\ v_s \approx 60\,P_0^{-0.60},\ v_p \approx 40\,P_0^{-0.57} \text{ and } T_{pinch(max)} \approx 20\,P_0^{-1.26}.$$

Using model parameters fitted from measured current waveforms we also computed the neutron yield versus pressure curve and found that the computed results curve has features of agreement with the measured curve of the Imperial College machine.

Keywords: Numerical experiment, dense plasma focus, Lee model code, neutron yield, axial velocity, radial trajectories

I. INTRODUCTION

The dense plasma focus machine can be used to study nuclear fusion in plasmas. To understand the performance of a plasma focus machine, the current trace [1], should be analysed because it contains information on the dynamic, electrodynamic, thermodynamic and radiation processes that occur in the various phases of the plasma focus [1-3]. One of the most important procedures therefore is to connect the numerical experiment [4] to the reality of the actual machine by fitting the computed current trace to a measured current trace [1, 5-11].

A. The 5-phase Lee Model Code

A brief description of the 5-phase model is given in the following.

The five phases (*a*-*e*) are summarised [4, 8-10, 12] as follows:

a. Axial Phase (see Figure 1 left part): Described by a snowplow model with an equation of motion which is coupled to a circuit equation. The equation of motion incorporates the axial phase model parameters: mass and current factors f_m and f_c. The mass swept-up factor f_m accounts for not only the porosity of the current sheet but also for the inclination of the moving current sheet shock front structure, boundary layer effects, and all other unspecified effects which have effects equivalent to increasing or reducing the amount of mass in the moving structure, during the axial phase. The current factor f_c accounts for the fraction of current effectively flowing in the moving structure (due to all effects such as current shedding at or near the back-wall, and current sheet inclination). This defines the fraction of current effectively driving the structure, during the axial phase.

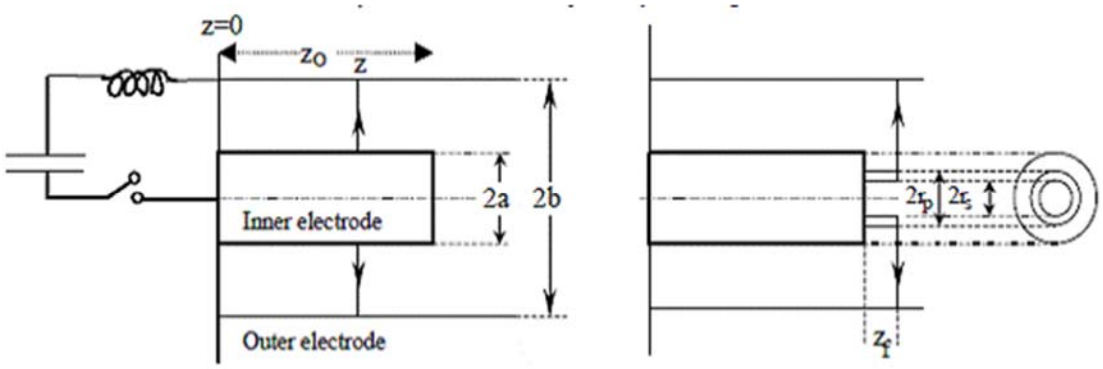

FIGURE 1. Schematic of the axial and radial phases. The left section depicts the axial phase, the right section the radial phase. In the left section, z is the effective position of the current sheath-shock front structure. In the right section r_s is the position of the inward moving shock front driven by the piston at position r_p. Between r_s and r_p is the radially imploding slug, elongating with a length z_f. The capacitor, static inductance and switch powering the plasma focus are shown for the axial phase schematic only.

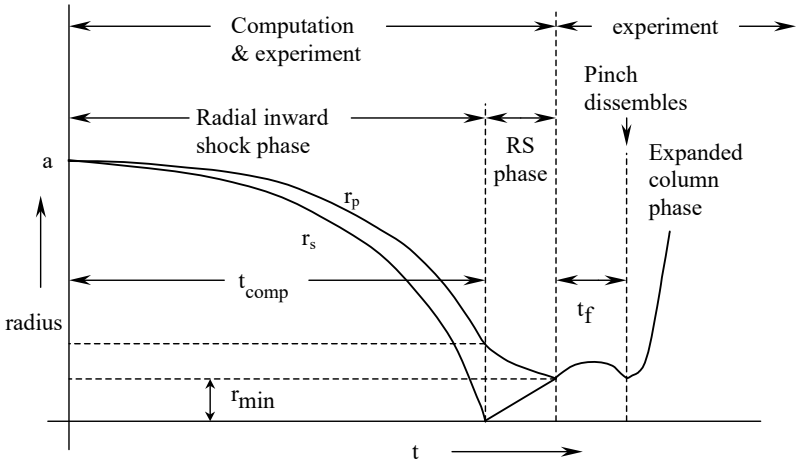

FIGURE 2. Schematic of radius vs time trajectories to illustrate the radial inward shock phase when r_s moves radially inwards, the reflected shock (RS) phase when the reflected shock moves radially outwards, until it hits the incoming piston r_p leading to the start of the pinch phase (t_f) and finally the expanded column phase.

b. Radial Inward Shock Phase (see Figure 1 right part, also Figure 2): Described by 4 coupled equations using an elongating slug model. The first equation computes the radial inward shock speed from the driving magnetic pressure. The second equation computes the axial elongation speed of the column. The third equation computes the speed of the current sheath, (magnetic piston), allowing the current sheath to separate from the shock front by applying an adiabatic approximation. The fourth is the circuit equation. Thermodynamic effects due to ionization and excitation are incorporated into these equations, these effects being particularly important for gases other than hydrogen and deuterium. Temperature and number densities are computed during this phase using shock-jump equations. A communication delay between shock front and current sheath due to the finite small disturbance speed is crucially implemented in this phase. The model parameters, radial phase mass swept-up and current factors f_{mr} and f_{cr} are incorporated in all three radial phases. The mass swept-up factor f_{mr} accounts for all mechanisms which have effects equivalent to increasing or reducing the amount of mass in the moving slug, during the radial phase. The current factor f_{cr} accounts for the fraction of current effectively flowing in the moving piston forming the back of the slug (due to all effects). This defines the fraction of current effectively driving the radial slug.

c. Radial Reflected Shock (RS) Phase (See Figure 2): When the shock front hits the axis, because the focus plasma is collisional, a reflected shock develops which moves radially outwards, whilst the radial current sheath piston continues to move inwards. Four coupled equations are also used to describe this phase, these being for the reflected shock moving radially outwards, the piston moving radially inwards, the elongation of the annular column and the circuit. The same model parameters f_{mr} and f_{cr} are used as in the previous radial phase. The plasma temperature behind the reflected shock undergoes a jump by a factor close to 2. Number densities are also computed using the reflected shock jump equations.

d. Slow Compression (Quiescent) or Pinch Phase (See Figure 2): When the out-going reflected shock hits the inward moving piston, the compression enters a radiative phase in which for gases such as neon, radiation emission may actually enhance the compression where we have included energy loss/gain terms from Joule heating and radiation losses into the piston equation of motion. Three coupled equations describe this phase; these being the piston radial motion equation, the pinch column elongation equation and the circuit equation, incorporating the same model parameters as in the previous two phases. The duration of this slow compression phase is set as the time of transit of small disturbances across the pinched plasma column. The computation of this phase is terminated at the end of this duration.

e. Expanded Column Phase: To simulate the current trace beyond this point we allow the column to suddenly attain the radius of the anode, and use the expanded column inductance for further integration. In this final phase the snow plow model is used, and two coupled equations are used similar to the axial phase above. This phase is not considered important as it occurs after the focus pinch.

II. PROCEDURE FOR NUMERICAL EXPERIMENT

From the published article, entitled "Table-top neutron source for characterization and calibration of dark matter detectors" [13], the machine parameters of the Imperial College

Plasma focus machine obtained are as follows. The Imperial College Plasma focus machine is a conventional Mather [14] type machine. The electrode structure of this machine consists of a copper anode tube 50 mm long, 20 mm in diameter while the outer cathode consists of eight, 10 mm diameter rods uniformly spaced coaxially at a diameter of 45 mm. The anode and cathode are separated by a pyrex glass tube enclosing 20 mm length of the anode. A triggered spark gap switch is connected to a 2.6 μF capacitor charged to 38 kV. This machine is operated at 2.62 Torr deuterium.

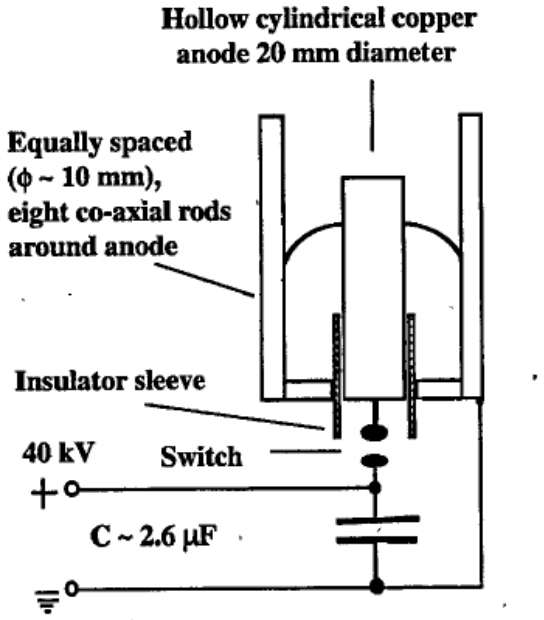

FIGURE 3.A schematic of Imperial College Plasma focus machine [15].

We digitised the published current derivative waveform of the plasma focus [13] using an open access source digitising program named Engauge [16]. The digitalised current derivative was then integrated with respect to time to obtain the current trace. We then used the Lee's 5 phase model code [4,12] (version: RADPF5.15) to configure the Imperial College Plasma focus machine by entering the following parameters:

Bank parameters:	inductance L_0, capacitance C_0 and stray circuit resistance r_0,
Tube parameters:	cathode radius b, anode radius 'a' and anode length z_0 and
Operational parameters:	voltage V_0 and pressure P_0 and the fill gas.

The computed total current waveform is fitted to the measured waveform by adjusting the model factors f_m, f_c, f_{mr} and f_{cr} [17-21] one by one, till the computed waveform agrees with the measured waveform.

First, f_m, f_c are tuned until (see Figure 4) the features (1) computed rising slope of the total current trace (2) rounding off of the peak current as well as (3) the peak current itself are in reasonable fit with the measured total current trace.

Then we continue to fit the radial f_{mr} and f_{cr} until the features (4) computed slope and (5) depth of the dip agree with the measured current trace. For the Lee Model 5-phase code the fitting ends here.

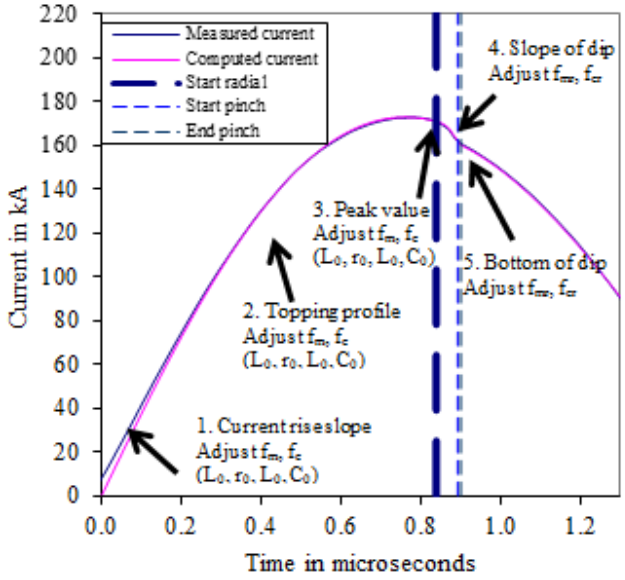

FIGURE 4. The 5-point fitting of current trace to the measured current trace obtained from Imperial College Plasma focus machine operated at 2.62 Torr in deuterium gas. The fitting uses Lee Model 5-phase code.

The machine, operation and fitting parameters are shown in Table-1

TABLE (1). Machine, operation and fitting parameters for the Imperial College Plasma focus machine used and fitted for this numerical experiment.

Capacitance C_0 (μF)	2.6
Static inductance L_0 (nH)	100
Circuit resistance r_0 (mΩ)	19.6
Cathode radius 'b' (cm)	2.25
Anode radius 'a'(cm)	1
Anode length 'z_0'(cm)	5
Charging voltage V_0 (kV)	38
Fill gas pressure P_0 (Torr)	2.62
Fill gas(molecular weight)	4
Fill gas(atomic number)	1
Fill gas(molecule(2))	2
Axial phase mass factor, f_m	0.15
Axial phase current factor, f_c	0.7
Radial phase mass factor, f_{mr}	0.16
Radial phase current factor, f_{cr}	0.7

III. RESULTS

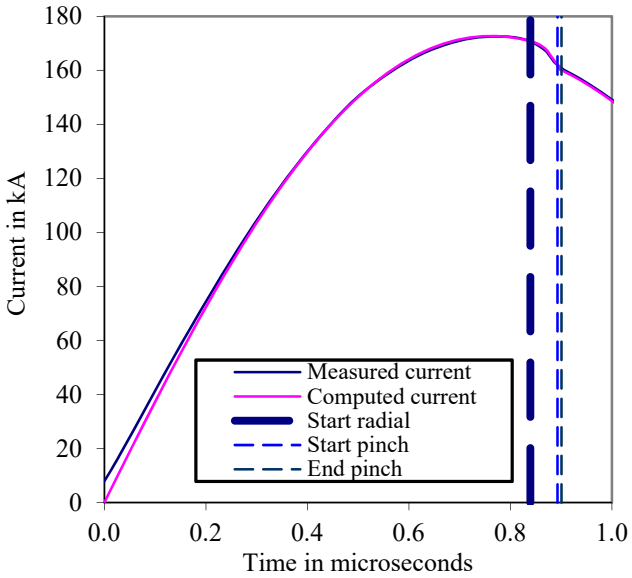

FIGURE 5. The measured current trace obtained from the current derivative of the Imperial College Plasma focus machine at 38 kV, 2.62 Torr deuterium gas [13] compared with computed current trace and correlated to the phases.

The computed and measured current traces in Figure 5 show a good fit. The peak current computed is 173 kA and exhibits a radial phase start time of 0.839 μs for pinch duration of 0.061 μs with a neutron yield of 6.6×10^6 n (The peak current obtained experimentally was 175 kA with a maximum neutron yield of $2.0 \pm 0.5 \times 10^7$ n at 2.62 Torr [13].) The computed values of the maximum pinch temperature, axial and radial speed as well as the neutron yield at 38 kV, 2.62 Torr deuterium gas are presented in Table-2.

TABLE (2). Information obtained from Lee's 5 phase model code configured for the Imperial College Plasma focus machine at 38 kV, 2.62 Torr deuterium gas.

Pinch maximum temperature (10^6 K)	7.5
Peak axial speed(cm/μs)	9.5
Peak radial shock speed(cm/μs)	37.1
Peak radial piston speed(cm/μs)	25.2
Neutron yield (10^6 n)	6.6

Using the machine operation and the fitted model parameters as shown in Table-1, the Imperial College Plasma focus machine is now configured at 38 kV, deuterium for pressure ranging from 0.5 Torr to 6.0 Torr to study the effect of the variation of pressure on maximum pinch temperature as well as the axial, radial and piston speeds. From the computed output we plotted Figures 6-9.

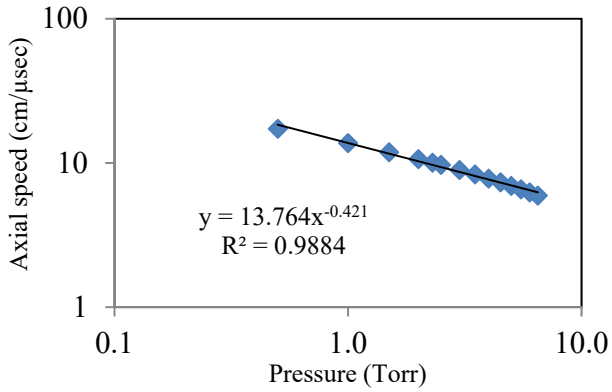

FIGURE 6. The variation of computed axial speed with respect to pressure operating at 38 kV in deuterium for the Imperial College Plasma focus machine.

When computed axial speed (v_a) was plotted in log scale against the variation in pressure P_0 as shown in Figure 6, we obtained the formula $v_a = 13.764 P_0^{-0.421}$ where the axial speed is in cm/µs while the pressure P_0 is in Torr. This can be approximated as $v_a \approx 14\, P_0^{-0.42}$. The computed axial phase of the Lee code uses an electromagnetic snowplow mechanism to compute the axial speed. Such a mechanism invariably produces an axial speed which is proportional to $(I/a)/P_0^{0.5}$; this quantity being known as S, the speed factor [22]. From this dependence it would seem at first sight that operating at the same voltage with the same anode radius one would expect that the axial speed being proportional to speed factor S should be proportional to pressure P_0 (the density ρ_0 being proportional to P_0). However the circuit equation is coupled to the current sheath motion through what is essentially the motor back electromotive force EMF effect. This back EMF effect requires that the faster the current sheath moves, the greater the back EMF which reduces the magnitude of the current. Thus as operational pressure is increased the circuit current increases due to slower current sheath speed. This provides a small compensation to the drop in speed due to the greater mass loading. This explains why the dependence of v_a with P_0 is not to the power of -0.5, but rather to a lesser power of -0.42.

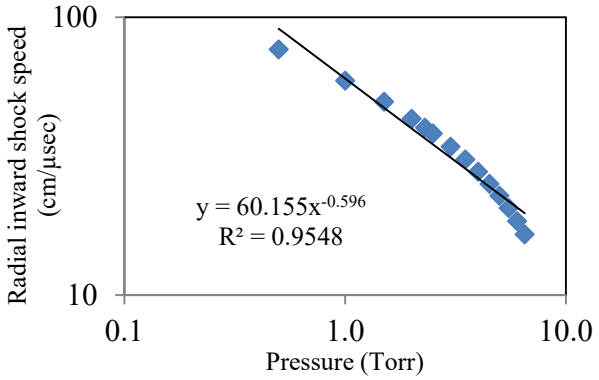

FIGURE 7. The variation of computed radial inward shock speed with respect to pressure operating at 38 kV in deuterium for the Imperial College Plasma focus machine

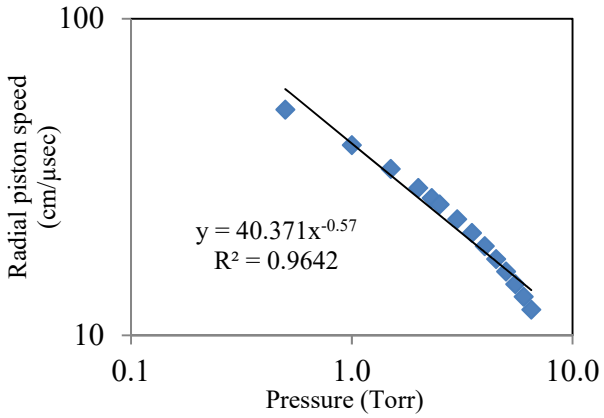

FIGURE 8. The variation of computed magnetic piston speed with respect to pressure operating at 38 kV in deuterium for the Imperial College Plasma focus machine

When computed radial inward shock speed (v_s) and radial piston speed (v_p) were individually plotted in log scale against P_0 as shown in Figures 7 and 8 respectively, we obtained the formula $v_s = 60.155P_0^{-0.596}$ and $v_p = 40.371P_0^{-0.57}$ respectively where the radial inward shock speed and radial piston speed are in cm/μs while the pressure P_0 is in Torr. This can be approximated as $v_s \approx 60\,P_0^{-0.60}$ and $v_p \approx 40\,P_0^{-0.57}$. The radial phase of the code uses an electromagnetic slug model mechanism to compute the radial speed [12]. The speed of the radial inward shock speed is determined by the magnetic pressure whereas the speed of the piston is determined by the first law of thermodynamics applied to the effective increase in volume between the shock front and the current sheet which is created by the incremental motion of the shock front.

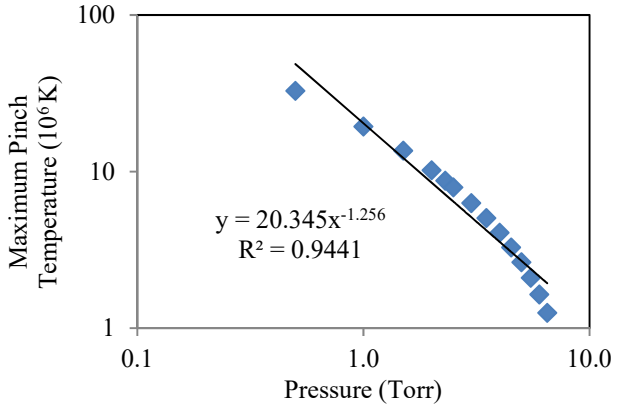

FIGURE 9. The variation of maximum pinch temperature with respect to pressure operating at 38 kV in deuterium for the Imperial College Plasma focus machine.

When the computed maximum pinch temperature ($T_{pinch\ (max)}$) was plotted in log scale against the variation in pressure P_0 as shown in Figure 9, we obtained the formula $T_{pinch\ (max)}=20.345\ P_0^{-1.256}$ where the pinch temperature is in 10^6K (10^6 Kelvin) and the pressure P_0 is in Torr. This

can be approximated as $T_{pinch(max)} \approx 20\, P_0^{-1.26}$. The detail explanation for this graph will be discussed in the next paragraph.

IV. DISCUSSIONS

Using the information obtained from the above Figures 6-9, it can be noted that as the pressure P_0 increases the axial speed v_a decreases. Similarly the radial shock speed v_s and the radial magnetic piston speed v_p also decreases. The decrease in the radial shock speed v_s causes a decrease in the temperature of the inward radial shock (the temperature depends on the shock speed to power of 2). This sets the stage for a decreased pinch temperature as pressure P_0 increases. As these two radial speed decreases, the time required for the radial reflected shock increases and also the pinch duration increases.

From Figure 6 we note that at around 4 Torr (at an axial speed around 5 cm/μs) there seems to be a gradual transition to a faster drop in speed than at lower pressures. This could be due to the transition from high Magnetic Reynold's Number (MRN) towards low MRN [23] or to a reduction in effective drive current due to the end of the axial phase being too far away from the time of the peak current for those higher pressure shots.

The radial shock speed is related to the axial speed by a predominantly geometrical factor which is about 2 for this plasma focus. Thus the same transition (to faster drop with P) is seen also in the behavior of the radial shock speed in Figure 7. The radial piston speed is related to the radial shock speed and a similar transition is seen in Figure 8 for the radial piston speed behaviour. The temperature (with a squared dependence on the radial shock speed) likewise shows the same, albeit accentuated, transition starting around 4 Torr.

When the measured and computed neutron yield versus variation in pressure P_0 were plotted as shown in Figure 10, the maximum computed neutron yield of 6.8×10^6 n occurred when the pressure was 2.3 Torr as compared to the maximum experimental yield of $2.0 \pm 0.5 \times 10^7$n that occurs at 2.6 Torr.

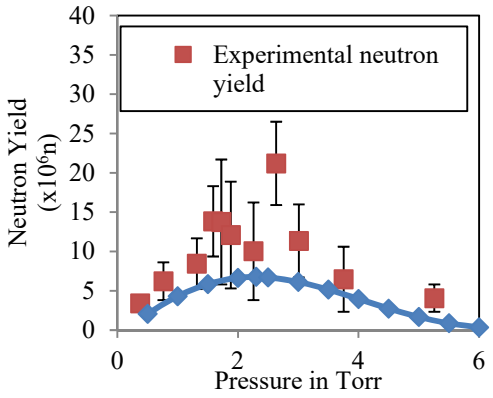

Figure 10. The variation of computed and experimental neutron yield with respect to pressure operating at 38 kV in deuterium for the Imperial College Plasma focus machine.

It should be noted that each point of the experimental value is the mean value while the error bars are the standard deviations. From Figure 10, it can be seen that the experimental and computed result are reasonably close (factor of 3 for the point showing the biggest difference); considering the high degree of variability recorded in the measurements.

V. CONCLUSIONS

From these numerical experiments, we conclude that for the Imperial College Plasma focus machine, the variation of operational pressure P_0 with axial speed v_a, radial shock speed v_s, piston speed v_p and pinch temperature has the relationship as shown below.

$$v_a \approx 14\, P_0^{-0.42},\ v_s \approx 60\, P_0^{-0.60},\ v_p \approx 40\, P_0^{-0.57} \text{ and } T_{pinch(max)} \approx 20\, P_0^{-1.26}.$$

The computed neutron yield results agree within a factor of 3 for the corresponding points with the published curves (F N Beg et al., 2002). Such agreement (of shape of curve and point by point values of computed versus measured values) is within the state of the art as no other model is able to estimate better than the correct order of magnitude of neutron yield. These results give confidence that the Lee model code gives a good guide to not just optimum neutron yields but also the behavior of neutron yield with pressure.

---

1. S. Lee and S. H. Saw, "The Plasma Focus- Scaling Properties to Scaling Laws". Joint ICTP-IAEA Workshop on Dense Magnetized Plasma and Plasma Diagnostics, (15 - 26 November 2010).
2. S. Lee, "Radiation in Plasma", edited by B.Namara. World Scientific, Singapore, 1984, Vol II, pp 978.
3. S. Lee, "In Laser and Plasma Technology", edited by S. Lee, B.C. Tan, C.S.Wong and A. C. Chew. World Scientific, Singapore, 1985, pp37, 64 and 387.
4. S. Lee, Radiative Dense Plasma Focus Computation Package: RADPF, 2014. http://www.plasmafocus.net http://www.plasmafocus.net/IPFS/modelpackage/File1RADPF.htm http://www.plasmafocus.net/IPFS/modelpackage/File2Theory.pdf http://www.plasmafocus.net/IPFS/modelpackage/UPF.htm;
5. S. Lee and S. H. Saw, *J. Fusion Energy* **27**, 292–295 (2008).
6. S. Lee, *Applied Physics Letters* **95**, 151503-3 (2009)
7. S. Lee, S. H. Saw, L. Soto, S. V. Springham and S. P. Moo, *Plasma Phys. Control. Fusion* **51**, 075006 -11 (2009).
8. S. H. Saw and S. Lee, *Energy and Power Engineering* **2**, 65-72 (2010).
9. S. Lee and S. H. Saw, *Energies* **3**, 711-737 (2010).
10. S. H. Saw and S. Lee, *Int. J. Energy Res.* **35**, 81–88 (2011).

11. S. Lee and S. H. Saw, *Int. J. Energ. Res.* **36**, 1366–1374 (2012).
12. S. Lee, *J Fusion Energy* **33**, 319-335 (2014).
13. F. N. Beg, I. Ross, A. Lorenz, J. F. Worley, A. E. Dangor and M. G. Haines, *Appl. Phys. Lett* **80**, 3009-3011 (2002).
14. J. W. Mather, Phys. *of Fluids* **3,** 134 (1960).
15. F. N. Beg, I. Ross, A. Lorenz, J. F. Worley, A. E. Dangor and M. G. Haines, *J. Appl. Phys* **88** , 3225-3230 (2000).
16. Website:http://sourceforge.net/project/showfiles.php?groupid=67696&package id=130007&release id=500277, 2009.
17. S. Lee, T. Y. Tou, S. P. Moo, M. A. Eissa, A. V. Gholap, K. H. Kwek, S. Mulyodrono, A. J. Smith, Suryadi, W. Usada and M. Zakaullah, *Am. J. Phys* **56**, 62–68 (1998).
18. T. Y. Tou, S. Lee and K. H. Kwek, IEEE *Trans Plasma Sci*, **17**, 311–315 (1989).
19. S. P. Chow, S. Lee and B. C. Tan, *J. of Plasma Phys* **8**, 21-31 (1972).
20. S. Al-Hawat, M. Akel , S. Lee and S. H. Saw, *J Fusion Energy* **31**, 13–20 (2012).
21. S. Lee, S. H. Saw, H. Hegazy, J. Ali, V. Damideh, N. Fatis, H. Kariri, A. Khubrani and A. Mahasi, *J Fusion Energy* **33**, 235-241 (2014).
22. S. Lee and A. Serban, *IEEE Transactions on Plasma Science* **23**, 1101-1105 (1996).
23. S. Lee, S. H. Saw, P. Lee, R. S. Rawat and K. Devi, *J Fusion Energy* **32**, 50-55 (2013).